L-Band and X-Band Antenna Design and Development for NeXtRAD

S. T. Paine, P. Cheng, D. W. O'Hagan, M. R. Inggs, H. D. Griffiths*, S. Alhuwaimel*

Dept. of Electrical Engineering, University of Cape Town, South Africa
*Dept. of Electronic and Electrical Engineering, University College London, UK
Email: daniel.ohagan@uct.ac.za

1. ABSTRACT

Research into multistatic, multi-band networked radar has resulted in the development of the NeXtRAD radar system. NeXtRAD has evolved from NetRAD and will be a fully polarimetric multistatic radar that operates in both X- and L-Band [1][2]. We provide an overview of the NeXtRAD system and discuss how it differs from its predecessor system, NetRAD. However, the main focus of this paper is on just an aspect of the novel NeXtRAD radar system, specifically the design and development of a dual polarised X-Band conical horn antenna as well as an L-Band prime focus parabolic dish antenna with centre frequencies of 8.5 GHz and 1.3 GHz respectively, and azimuth beamwidths of 10°. The X-Band antenna is required to handle a peak power of 400 W while the L-Band antenna must be capable of 1.5 kW, as well as low windage to allow mounting on a tripod. An off-the-shelf antenna meeting the aforementioned specifications was either not available or unaffordable, and this has led the authors to develop their own solution to meet requirements. The antennas have been simulated using FEKO [3] and CST [4] and the manufactured prototypes comply well with simulated results. The manufactured X-Band antenna prototype was found to have an azimuth HPBW of 9.1° and 10.4° when horizontally and vertically polarised respectively which agrees well with the corresponding FEKO simulated values of 9.3° and 10.7°. Similarly, the manufactured L-Band prototype antenna was found to have an azimuth HPBW 13.9° and 12.4° when horizontally and vertically polarised respectively – also agreeing well with the FEKO simulated HPBW of 13.9° and 12.1° respectively. The antennas reported in this paper have been developed from conveniently accessible components/materials such as sheet aluminium, a modified parabolic reflector and a circular waveguide feed (paint-tin) that accommodates two probe-pins for both polarisations.

2. INTRODUCTION

The University of Cape Town (UCT) together with University College London (UCL) are in the process of building a multistatic networked radar system that aims to improve on a previous radar system known as NetRAD. NetRAD was originally developed by UCL and UCT [1]. To improve upon NetRAD, NeXtRAD has been designed to utilise two frequency bands as opposed to one, namely L-Band ($f_0 = 1.3$ GHz) and X-Band ($f_0 = 8.5$ GHz) and will also be fully polarimetric.

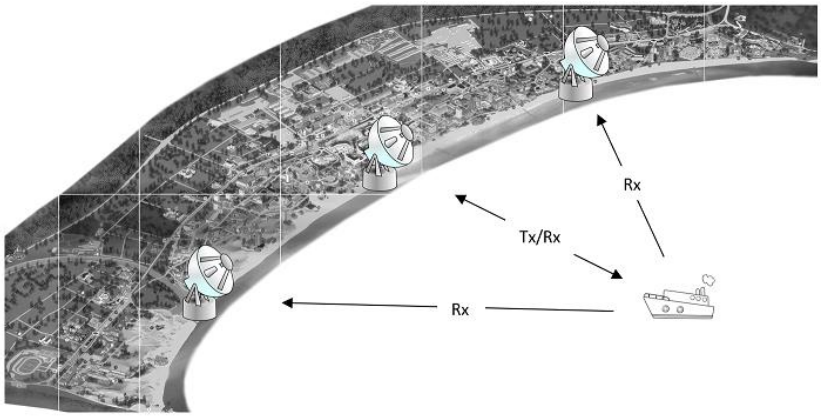

Figure 1: NeXtRAD antenna layout with central Tx/Rx node and two passive Rx-only flanking nodes [2].

Figure 1 shows the basic node geometry of the NeXtRAD system. One of the key features of the NeXtRAD system is that it is able to operate in both X- and L-Band, switching between both planes of polarisation as required. The central active node will transmit either a horizontally or vertically polarised pulse in either X- or L-Band, while the target echo can be received by all three nodes in either horizontal or vertical polarisation.

Multistatic, polarimetric, measurements of clutter and targets are very scarce. Obtaining quality measurement data and performing analysis is therefore the first step towards building suitable prediction models for this new generation of networked, polarimetric radars that operate bistatically and multistatically. Polarimetry is, of course, very well understood, especially in the field of imaging radar. However, most of the models used are based on monostatic SAR systems, so NeXtRAD will be an important testbed for theoretical modelling for bistatic and multistatic SAR.

There are two types of polarimetric radar i.e. full polarimetric systems (the full scattering matrix is gathered) versus hydbrid systems. The latter use circular polarisation for transmit (for example), and receive two linear polarisations. There is much disagreement in the imaging radar community as to whether a compact polarimetric system can be properly calibrated and provides useful data that discriminates objects sufficiently well. NeXtRAD will be making a contribution here. We point out that the hybrid system leads to significant system cost reduction, since the transmitter can be fed via a hybrid coupler directly to the transmit antenna, without the need for high power switches.

3. L-BAND PARABOLIC DISH ANTENNA DESIGN

The design and manufacture of a dual polarised L-Band dish antenna for use in NeXtRAD is presented. The manufactured antenna has been tested and compared with the FEKO and CST simulated models and illustrate the feasibility of the design for use in NeXtRAD.

3.1 L-Band Application Requirements

- Dual polarised (Horizontal and Vertical)
- L-Band with centre frequency of $f_0 = 1.3$ GHz
- Minimum 50 MHz bandwidth
- 10° azimuth HPBW
- 1.5 kW peak power handling capabilities
- Be able to be mounted on a standard tripod and withstand harsh environmental conditions such as strong winds

To meet these application requirements, a bespoke antenna has had to be designed as no off-the shelf solution was available that met the strict requirements.

3.2 Feed Design

Prior work by the authors has found that using a circular waveguide can improve port-to-port isolation by as much as 8 dB over an equivalent square waveguide [5]. In addition to the performance advantages achieved through the use of a circular feed, it also has the advantage of being simpler to manufacture. Certain tin cans can be used to make a circular waveguide such as with MIT's innovative "Coffee Can Radar" [6][7][8].

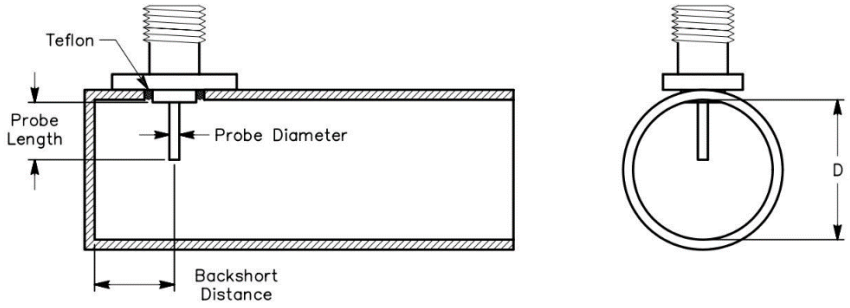

Figure 2: (Left) Side view and (Right) front view of a circular waveguide illustrating the basic probe placement parameters [8].

Figure 2 shows the schematic of a circular waveguide. Feed blockage plays a major role in determining the overall performance of an antenna, especially in the case of an electrically small dish antenna (where $D < 10\lambda_0$) [9]. As the required antenna is approximately $7\lambda_0$ in diameter, it has been decided that an open ended waveguide feed with no flair would be used as this will keep feed blockage to a minimum. The cut-off wavelength, λ_c, can be related to the diameter, D, of the waveguide as [6][8]:

$$D = \frac{C}{1.705 \times f_c} \tag{1}$$

The waveguide in question is required to operate at L-Band ($f_0 = 1.3$ GHz) which has a lower cut-off frequency of 1 GHz. This resulted in a diameter size of 176 mm. After searching for an appropriate cylinder, it has been found that a 5 litre paint tin has an inner diameter 175 mm and a length of 230 mm (almost exactly λ_0) and is adequate for use as a waveguide at the desired L-Band frequencies. Another aspect to consider when designing a waveguide is the coaxial to waveguide transition.

Looking at Figure 2, it can be seen that the inset probe is a simple quarter wavelength monopole radiator [8][10]. The length of the probe required for a centre frequency of 1.3 GHz is defined as:

$$L_{probe} = \frac{\lambda_0}{4} = \frac{C}{4f_c} = 57.7\ mm \tag{2}$$

The backshort distance is defined as the distance from the probe to the back-wall of the waveguide.

$$\lambda_g = \frac{\lambda_0}{\sqrt{1 - \left(\frac{\lambda_0}{1.705 \times D}\right)^2}} \approx 360\ mm \tag{3}$$

$$\therefore L_{backshort} = \frac{\lambda_g}{4} \approx 90\ mm \tag{4}$$

3.3 Truncated Reflector Design

The requirements state that the beamwidth in the azimuth plane must be 10°. The requirements on the elevation plane beamwidth are slightly more flexible and therefore the antenna diameter can be reduced in the elevation plane. It has therefore been decided that the edge taper for the vertical plane would be at the -3 dB point as opposed to the horizontal edge taper which is designed to be at the -10 dB point (i.e., the 90% radiation efficiency level).

The azimuth HPBW of the paint can feed has been determined through FEKO simulation to be 90° when horizontally polarised and 107° when vertically polarised. The f/D ratio for the vertical section of the antenna must therefore be between $0.5 \leq f/D \leq 0.6$ in order to meet the illumination taper requirements mentioned.

The focal point cannot change between the vertical and horizontal dimension of the dish and therefore the appropriate height of the antenna can be calculated as:

$$D_{vertical} = \frac{465}{0.6} = 775\ mm \tag{5}$$

Using the FEKO determined diameter of 1500 mm, the truncated dish antenna has been simulated and further optimised using FEKO. Table 1 summarises the performance characteristics of both the calculated and FEKO iterated final result for the truncated dish antenna. It can be seen from Table 1 that while the FEKO optimised and the designed antenna characteristics are very similar, in some cases within a dB of each other, well within the margin for error, the goal has been to design the antenna to be as compact as practicably possible and this has been achieved in the optimised design.

Table 1: Simulated antenna performance characteristics for both the calculated and FEKO iterated final result for the truncated dish antenna.

Parameter	Initial	Optimised Final
Diameter	1500 mm	1440 mm
Height	775 mm	744 mm
Depth	302.4 mm	290.3 mm
Focal Point	465 mm	446 mm
f/D ratio	0.31	0.31
Parabolic Equation	$y = (5.38 \times 10^{-4})x^2$	$y = (5.60 \times 10^{-4})x^2$
HPBW (Az)	H-Pol - 9.8° V-Pol - 9.2°	H-Pol - 10.7° V-Pol - 10.0°
HPBW (El)	H-Pol - 15.5° V-Pol - 15.7°	H-Pol - 16.4° V-Pol - 16.6°
SLL (Az)	H-Pol - 20.3 dB V-Pol - 17.1 dB	H-Pol - 20.3 dB V-Pol - 16.9 dB
SLL (El)	H-Pol - 15.0 dB V-Pol - 13.9 dB	H-Pol - 15.1 dB V-Pol - 15.0 dB
F/B ratio	H-Pol - 25.1 dB V-Pol - 27.0 dB	H-Pol - 24.7 dB V-Pol - 30.7 dB

3.4 Antenna Manufacturing

A modified version of the pre-fabricated antenna has been designed and optimised through simulations. The antenna was then manufactured and tested to illustrate that the simulations are accurate enough to warrant further manufacturing expense. The largest 2.45 GHz off-the-shelf antenna was purchased and the beam pattern and resultant HPBW were confirmed through testing. The purchased antenna was then modified through physical extension to make it conform to the design requirements. Finally, the modified antenna was simulated and the results appear in Table 2.

Table 2: Simulated antenna performance characteristics for the modified antenna.

Parameter	Final Optimised
Diameter	1350 mm
Height	600 mm
Depth	370 mm
Focal Point	307.85 mm
f/D ratio	0.23
Parabolic Equation	$y = (8.16 \times 10^{-4})x^2$
HPBW (Az)	H-Pol - 13.9° V-Pol - 12.1°
HPBW (El)	H-Pol - 19.7° V-Pol - 20.5°
SLL (Az)	H-Pol - 17.4 dB V-Pol - 17.4 dB
SLL (El)	H-Pol - 16.3 dB V-Pol - 15.2 dB

The purchased antenna consisted of two sections that were bolted together in the middle. To extend the dish to the required diameter, 3 mm thick aluminium flat strips were used to join the two sections of the parabolic reflector. Once the skeletal shape had been completed, a wire mesh was placed over the entire surface of the reflector. The modified section attempted to maintain the parabolic profile of the reflector, but was not fully conformist.

Once the antenna structure had been manufactured and its new dimensions confirmed, the waveguide feed was built using a 1 litre paint tin. The feed probes were then measured and cut slightly longer than the designed length. This allowed for adjustments to be made by cutting the probe smaller during testing. The probes were inserted and the waveguide placed onto the wooden support structure such that the waveguide phase centre sits at the dish focal point. Figure 3 shows the completed prototype antenna. Once the antenna prototype had been manufactured, the antenna was tested and the results compared to the simulated results.

Figure 3: Prototype antenna with dual polarised waveguide feed mounted to a tripod for testing.

3.5 S-Parameter Measurements

The S-Parameters were simulated using CST and both the simulated and measured results are shown in Figure 4 where it can be seen that the antenna feed performs relatively closely to the simulated results. It was found that the antenna feed had an $S_{11/22}$ measurement of below -15 dB across the entire specified bandwidth whilst also maintaining an S_{21} isolation between planes of polarisation of greater than -15 dB across the specified bandwidth. The S_{22} measurements have been omitted due to their similarity to the S_{11} measurements.

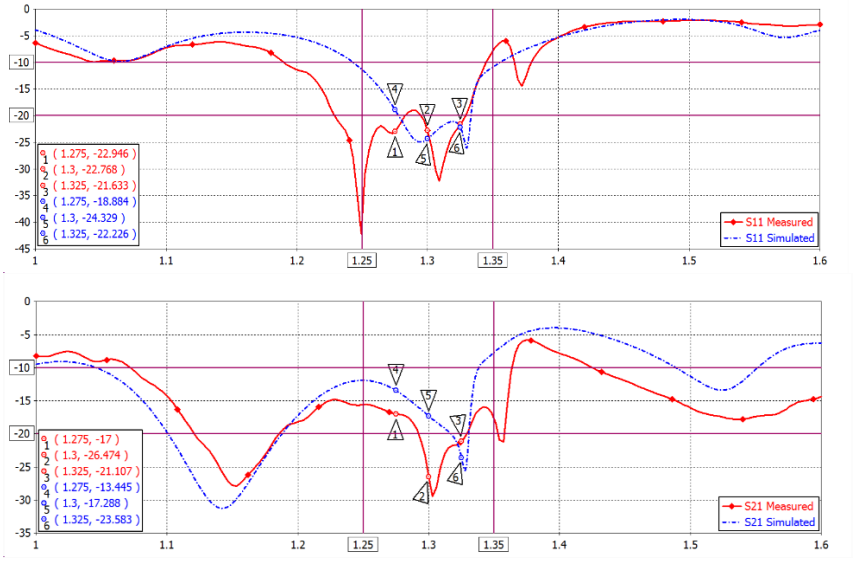

Figure 4: Measured (Red solid) versus simulated (Blue dashed) S_{11} (top) and S_{21} (bottom) parameters for the dual polarised feed with the phase centre of the feed at the focal point of the antenna.

3.6 Beam Pattern Measurements

The azimuth and elevation radiation patterns of the antenna were measured in each plane of polarisation and the results are summarised in Table 3. It can be seen from the polar plots in Figure 9 in Appendix A that the measured results closely align with the simulated results. The measured results are slightly offset due to the method of plotting the data, however, it can be seen that the antenna performs as designed.

Table 3: Summary of measured prototype antenna results.

Measured Parameters	Horizontal Polarisation	Vertical Polarisation
Azimuth HPBW	12.4°	13.9°
Elevation HPBW	20.0°	19.6°
Azimuth SLL	17.4 dB	16.4 dB
Elevation SLL	15.7 dB	15.8 dB

4. X-BAND ANTENNA DESIGN

The X-band requirements are very similar to that of L-Band with 10° azimuth HPBW in both polarisations. The only difference being the operating frequency is 8.5 GHz and a power handling capability of 400 W. This section covers the design procedure, prototype, testing, and results.

4.1 Design Procedure

Much like the L-Band antenna, a circular waveguide and conical horn antenna have been chosen as the most readily feasible solutions for dual polarisation due to their symmetrical structure, ease of fabrication, and the availability of equipment and facilities at UCT. In our case, the freespace wavelength, λ_0, is 35.29 mm. The design of the horn antenna reduces the HPBW and increase the gain.

4.2 Dual-Polarised Waveguide Design

The X-band circular waveguide and dual polarised feeds can be designed in the same way as described in Section 3.2. A standard sized water pipe with an inner diameter of 28 mm has been chosen for the circular waveguide section. Using (1), the cutoff frequency of the fundamental T_{11} mode was found to be 6.28 GHz. Therefore, the operating frequency was above the cutoff frequency of the T_{11} mode.

For an X-band circular waveguide, with the values $\lambda_0 = 35.29$ mm and $\lambda_c = 47.77$ mm, the waveguide wavelength λ_g has been found to be 53.36 mm from (3). Equations (2) and (4) have been used to find the length of the probe (L_{probe}) and backshort ($L_{backshort}$), and these have been found to be 8.82 mm and 13.09 mm respectively.

The dual polarised waveguide has been constructed by inserting two probes orthogonal to each other. The horn antenna has been designed to flare the waveguide aperture to increase the aperture size, reduce the HPBW and increase the antenna gain.

4.3 Conical Horn Antenna Design

Figure 5 shows the side view of a horn antenna and the relevant variable lengths.

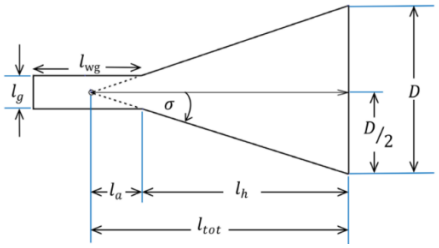

Figure 5: Side view of the waveguide and horn antenna

For the required HPBW θ of 10°, the diameter of the antenna aperture (D) is calcuated to be 247.06 mm using [11][12]:

$$D = \frac{70\lambda_\circ}{\theta} \tag{6}$$

The length of the horn l_h is equal to 511.14 mm using [12]:

$$l_h = \frac{D^2}{3\lambda_\circ}\left(1 - \frac{l_g}{D}\right) \tag{7}$$

The length of the waveguide (l_{wg}) is set to 50 mm which allows EM waves to settle and attenuate all the other higher-order modes.

4.4 Fabrication and Testing

Due to physical constraints, the dimensions were slightly altered to those shown in Table 4. The length of the probe has been adjusted to better match the impedances from coaxial line to waveguide.

Table 4: Dimensions of the circular waveguide and conical horn after fabrication.

Circular waveguide	l_g	28 mm in diameter
	L_{probe}	11 mm
	$L_{backshort}$	14 mm
	l_{wg}	50 mm
Conical horn	l_h	510 mm
	D	248 mm in diameter

Figure 6 shows the fabricated antenna prototype with the dual polarised waveguide and conical horn antenna.

Figure 6: Prototype conical horn with dual polarised waveguide.

The radiation patterns have been measured on the rooftop of Menzies Engineering Building at UCT. All of the recorded data have been plotted in MATLAB for analysis. The results obtained from the prototype experiments and the FEKO simulations have been compared.

4.5 Results

This section shows the experimental measurements and the FEKO simulated measurements. These include the S-parameter measurements and radiation pattern plots measuring the HPBWs and SLLs. The FEKO result includes the modified and revised version.

4.5.1 S-Parameters

The reflection coefficient of Port 1 is measured as S_{11}, Port 2 as S_{22}, and the transmission coefficient or isolation as S_{12}. The parameter S_{21} has been neglected due to being the same as S_{12}.

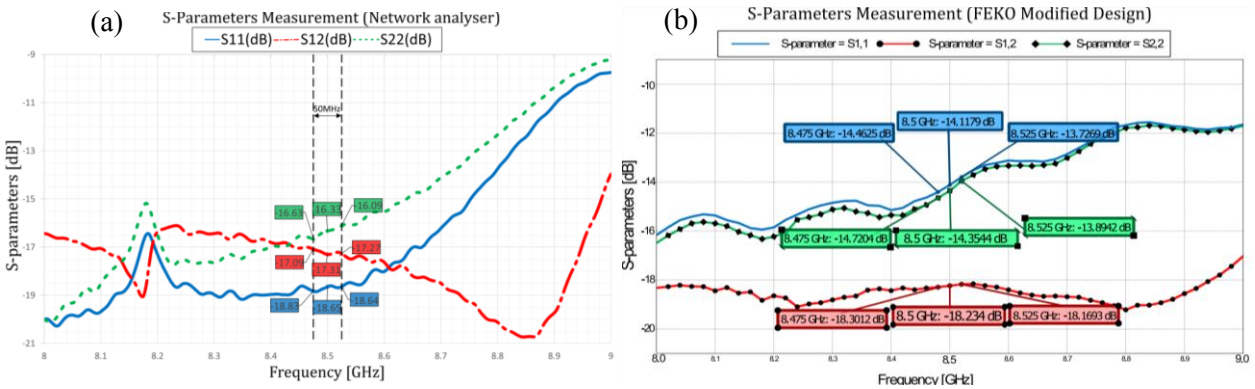

Figure 7: S-parameter plots of S_{11}, S_{12}, and S_{22} at the frequency range of 8 GHz to 9 GHz. (a) Prototyped antenna. (b) FEKO simulation.

In Figure 7(a), for the experimental S-parameters at 8.5 GHz, the reflection coefficients S_{11} and S_{22} are -18.65 dB and -16.33 dB respectively. The antenna achieved an isolation S_{12} of -17.31 dB, implying that when one of the ports is transmitting, only 1.86% of the transmitting power is being received by the other port.

In Figure 7(b), the modified FEKO S-parameter measurement shows all three plots are below -14 dB at 8.5 GHz, implying that more than 90% of the power is being radiated and that there is less than 2% leakage between the two ports. Analysing the 50 MHz instantaneous bandwidth from Figure 7, the measurements are similar to their respective 8.5 GHz measurements. Therefore, the antenna yields an efficient response at 8.5 GHz $\pm$ 25 MHz.

4.5.2. Radiation Patterns

The radiation patterns in Figure 8 are the results of measurements performed on the roof of the UCT Engineering Building alongside the corresponding FEKO simulations. Both elevation and azimuth planes of the radiation pattern have been plotted and summarised in Figure 8.

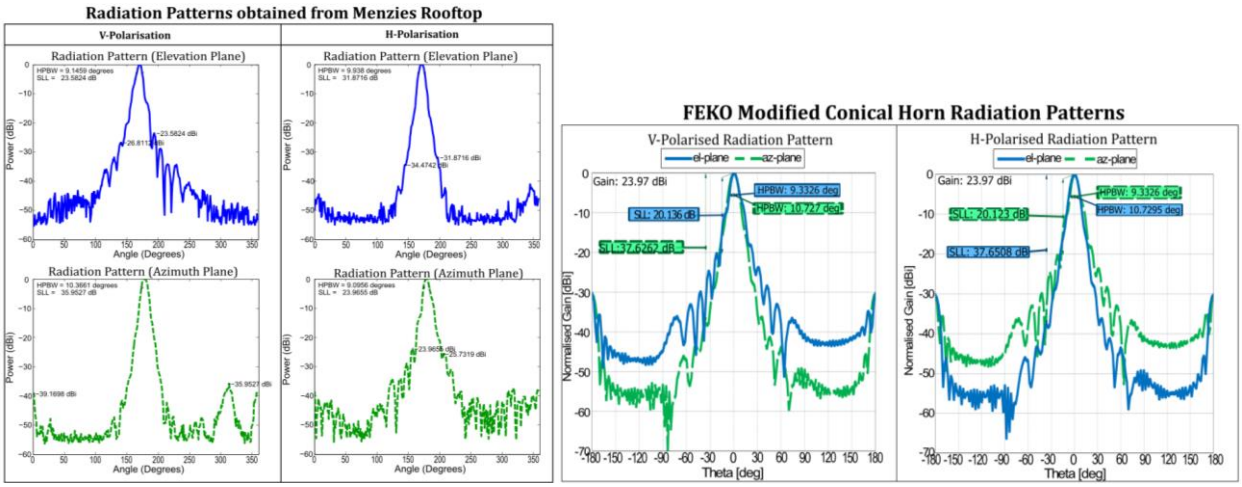

Figure 8: Radiation pattern measurements including both polarisations in both planes, HPBW and SLL measurements. (Left) Prototyped antenna. (Right) FEKO simulation.

The HPBWs for all the measurements achieved approximately $10° \pm 1°$ in both planes of polarisation. The peak-to-sidelobe level (PSLL) for the measurements were almost all greater than 20 dB. Furthermore, the HPBWs and SLLs of the prototype and the FEKO modified design were closely matched. This confirms that the dual polarised conical horn antenna is functional and that the FEKO generated simulations are of high fidelity.

5. CONCLUSION

The simulated results have shown a close agreement to the measured results. Table 5 and Table 6 summarise the results found in both the FEKO and CST simulations as well as the measured results for the L-Band and X-Band designs respectively. The measured antenna results showed an azimuth HPBW of 12.4° and 13.9° when horizontally and vertically polarised respectively. These results are within the 0.5° margin of error introduced into the measurements due to the measurement technique.

Table 5 confirms what can be seen in Figure 9, that the measured results closely match the simulated results from both FEKO and CST. From this, it is concluded that while the azimuth beamwidth in each plane of polarisation is greater than the required 10°, the prototype antenna performs as designed and simulated.

The S-parameter simulations have been found to be accurate and reliable for all test cases. In the L-Band case, deviations between the simulated and measured S-parameters have been found when the feed is attached to the focal point of the dish antenna. These deviations can be attributed to inconsistent mesh shape and because the aluminium strips do not perfectly conform to the parabolic profile of the reflector.

From the measurement results, it has been shown that manufacturing tolerances are critical to the performance of the antenna. Operating to stricter engineering tolerances can ensure that the final manufactured solution can meet the specified performance requirements for NeXtRAD.

Table 5: L-Band comparison of results between FEKO simulations and prototype antenna measurements.

	Horizontal Pol		Vertical Pol	
	Simulated	Measured	Simulated	Measured
Az HPBW	12.1°	12.4°	13.9°	13.9°
El HPBW	20.5°	20.0°	19.7°	19.6°
Az SLL	-17.3 dB	-17.4 dB	-17.4 dB	-16.4 dB
El SLL	-15.2 dB	-15.7 dB	-16.3 dB	-15.8 dB

Table 6: X-Band comparison of results between FEKO simulations and prototype antenna measurements.

	Horizontal Pol		Vertical Pol	
	Simulated	Measured	Simulated	Measured
Az HPBW	9.3°	9.1°	10.7°	10.4°
El HPBW	10.7°	10.0°	9.3°	9.2°
Az SLL	-20.1 dB	-23.8 dB	-37.6 dB	-35.9 dB
El SLL	-37.7 dB	-31.9 dB	-20.1 dB	-23.6 dB

6. ACKNOWLEDGEMENTS

The NeXtRAD consortium acknowledge the support of the Royal Academy of Engineering, the IET A.F. Harvey Prize, the Engineering and Physical Sciences Research Council, the Office of Naval Research, KACST, FFI (Norway) and the South African NRF and DoD (Project Ledger) in this work. Michael Inggs obtained the substantial grant for NeXtRAD from the RSA NRF.

7. REFERENCES

[1] S. R. Doughty, "Development and performance evaluation of a multistatic radar system," Ph.D. dissertation, University College London, 2008.

[2] M. Inggs, H. Griffiths, F. Fioranelli, M. Ritchie, and K. Woodbridge, "Multistatic radar: System requirements and experimental validation," *SEE Int. Radar Conference RADAR 2014, Lille, 13-17 Oct. 2014.*

[3] Altier, "FEKO," 2015, accessed: 2016-01-18. [Online]. Available: https://www.feko.info/product-detail/overview-of-feko

[4] CST Studio, "CST Studio Suite 2015," 2015, accessed: May 25, 2016. [Online]. Available: https://www.cst.com/Content/Articles/article909/CST-STUDIO-SUITE-2015.pdf

[5] S. Paine, "Design and Implementation of Dual Polarised L-Band Parabolic Dish Antenna for NeXtRAD," University of Cape Town, Cape Town, MSc Dissertation, 2016.

[6] Gregory Charvat, Jonathan Williams, Alan Fenn, Steve Kogon, and Jeffrey Herd, "Build a small radar system capable of sensing range, doppler, and synthetic aperture radar imaging," (Massachusetts Institute of Technology: MIT), accessed: June 13, 2015. [Online]. Available: http://ocw.mit.edu

[7] G. L. Charvat, "MIT IAP 2011 Laptop Based Radar: Block Diagram, Schematics, Bill of Material, and Fabrication Instructions," *Presented at the 2011 MIT Independent Activities Period (IAP)*, pp. 1–51, 2012.

[8] P. Wade, "Understanding Circular Waveguide - Experimentally," 2001, accessed: November 27, 2015. [Online]. Available: http://www.w1ghz.org/QEX/circular wg.pdf

[9] ——, "Parabolic Dish Feeds," 1998, accessed: May 25, 2016. [Online]. Available: http://www.w1ghz.org/antbook/chap11.pdf

[10] C. A. Balanis, *Antenna Theory: Analysis and Design*, 3rd ed. New York: John Wiley & Sons, Inc., 2011.

[11] B. Downing, "Microwave Components and Antennas," EEE5121Z Lecture notes, Department of Electrical Engineering, University of Cape Town, South Africa, 2014.

[12] O. Daniyan, F. Opara, and et al., "Horn Antenna Design: The Concepts and Considerations," IJETAE, vol. 4, no. 5, pp. 706–708, July May 2014, accessed: November 25, 2015. [Online]. Available: http://www.ijetae.com/files/Volume4Issue5/IJETAE 0514 107.pdf

8. APPENDIX A

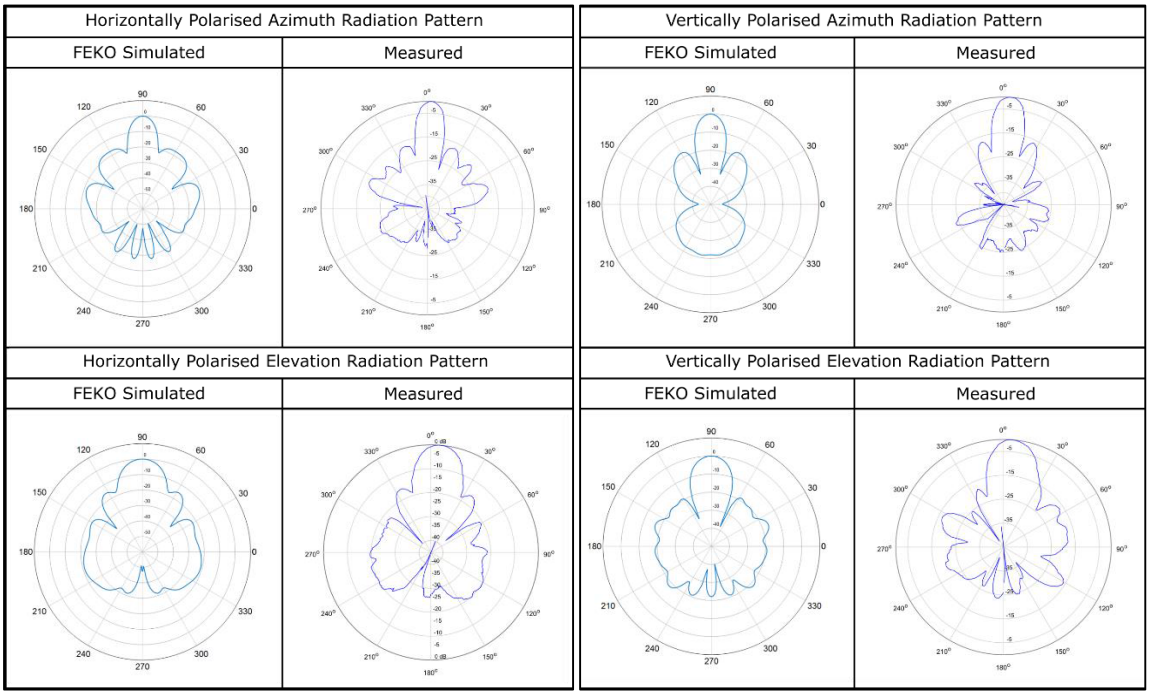

Figure 9: (Left) Horizontally polarised (Right) Vertically polarised measured vs simulated beam patterns.